How to cite: *Angew. Chem. Int. Ed.* **2025**, e202504396
doi.org/10.1002/anie.202504396

Organic Materials

Constructing Biomimetic Channels in Hydrogen-Bonded Organic Framework via Post-Synthesis for Enhanced Proton Conductivity

Yu-Lin Li[+], Jiang-Feng Lu[+], Qi Yin, Lei Cai, Hui-Jie Jiang, Chen Liu, Gang Xu, and Tian-Fu Liu**

Abstract: Proton transport channels in biological systems are constructed by the specific amino acid residues with hanging carboxylic acid groups acting as proton donors and acceptors, enabling rapid proton conduction via the Grotthuss mechanism. Hydrogen-bonded organic frameworks (HOFs) are promising candidates for artificially simulating proton channels due to their designable structure and abundant proton sources in the network. However, these protons were usually immobilized within hydrogen bonds between two building blocks, which require a high energy barrier for initiating proton transport. Post-synthetic modification (PSM) may be a viable solution to the above problems but has yet to be achieved in HOFs. Herein, we demonstrate for the first time that unoccupied carboxylic acid groups can be created through post-synthesis which further stabilizes water molecules to construct continuous proton channels, bringing boosted proton conductivity by three orders of magnitude. The structure transformation process and the intermediate can be identified clearly by crystallography with an unveiled mechanism. This work offers a new approach to constructing biomimetic channels for proton conduction and HOF functionalization.

Proton transport channels in biological systems play essential roles in processes such as energy metabolism, signal transduction, and ion balance maintenance.[1–3] These channels were composed of polypeptide chains with amino acid residues precisely arranged for proton conduction. For example, in cytochrome C oxidase (CcO), a key enzyme complex in the mitochondrial respiratory chain, the proton channel features a cavity lined with polar amino acid residues of aspartic acid and glutamic acid, and water molecules (upper left part of Figure 1).[4] Protons are efficiently transported via the hydrogen-bond network established by water molecules and the carboxylic acid groups on the amino acid side chains.[5–8] Artificially replicating such structures for biosensing and biomedical applications is highly valuable but a significant challenge.[9]

Hydrogen-bonded organic frameworks (HOFs) have emerged as promising candidates for the design of biomimetic materials due to their highly ordered structure, abundant proton source, and structural tunability.[9–13] However, in most HOFs, protons are immobilized in the hydrogen bonds between adjacent monomers,[14–19] which require high energy barrier to initiate the release of protons and the subsequent transport (bond energy ~40 kcal mol^{-1}), limiting their availability for proton conduction. Post-synthetic modification (PSM) is an effective approach to realize the customized structure and improve the performance of molecular-based materials.[20,21] However, executing PSM in HOFs is very challenging and has yet to be achieved due to the fragile hydrogen bonds and the ease of structure collapse. Inspired by the generation of aspartic acid through succinimide-mediated deamidation in very mild conditions of water without requiring acidic or basic catalysts (upper right part of Figure 1),[22–24] we employed the same method to produce free carboxylic acids for enhanced proton transport. Specifically, we chose pyromellitic diimide (PDI), a linear imide molecule, as building blocks and combined it with a triangular molecular melamine to construct a hydrogen-bonded organic framework designed as PFC-49 (PFC = porous materials from FJIRSM, CAS). In the presence of water, PDI molecules underwent a ring-opening deamidation reaction and initiated a structural transformation from PFC-49 to PFC-50, which not only created penetrated 1D channels but also created ordered carboxylic acids on the pore surfaces. These exposed carboxylic acids further stabilized the water molecules and formed proton transport channels, similar to that observed in CcO. Consequently, the proton conductivity of PFC-50 improved by three orders of magnitude compared to PFC-49.

Synthesis and structural transformation of PFC-49 and PFC-50. Colorless bulk crystals of PFC-49 were obtained in dimethylformamide (DMF) solution of PDI and melamine at 90 °C for 7 days. Single crystal X-ray structure determination

[*] Y.-L. Li[+], J.-F. Lu[+], Q. Yin, L. Cai, H.-J. Jiang, C. Liu, G. Xu, T.-F. Liu
State Key Laboratory of Structural Chemistry, Fujian Provincial Key Laboratory of Materials and Techniques toward Hydrogen Energy, Fujian Institute of Research on the Structure of Matter, Chinese Academy of Sciences (CAS), Fuzhou 350002, China
E-mail: gxu@fjirsm.ac.cn
tfliu@fjirsm.ac.cn
Y.-L. Li[+], T.-F. Liu
University of Chinese Academy of Sciences, Beijing 100049, China
J.-F. Lu[+], G. Xu, T.-F. Liu
Fujian Science Technology Innovation Laboratory for Optoelectronic Information of China, Fuzhou 350108, China
[+] These authors contributed equally to this work.

Additional supporting information can be found online in the Supporting Information section

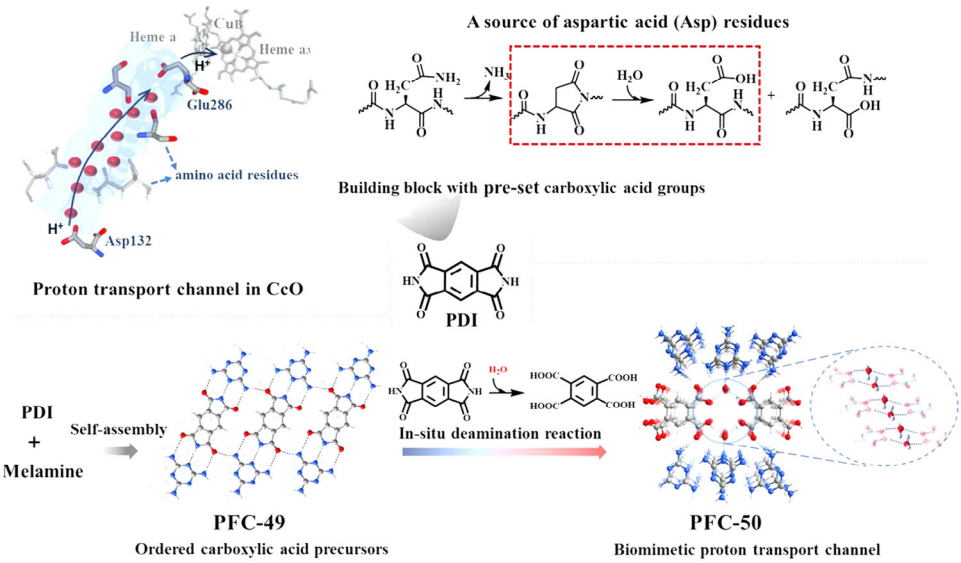

Figure 1. Upper left: The proton transport D-channel in CcO is composed of amino acid residues and water molecules (magenta spheres). Upper right: Succinimide-mediated deamidation reaction as the source of asparagine residues. Lower panel: The schematic illustration of the synthesis and structural transformation process of PFC-49 and PFC-50. The partial zoom highlights the 1D water channel stabilized by exposed carboxylic acids along the *a*-axis in PFC-50.

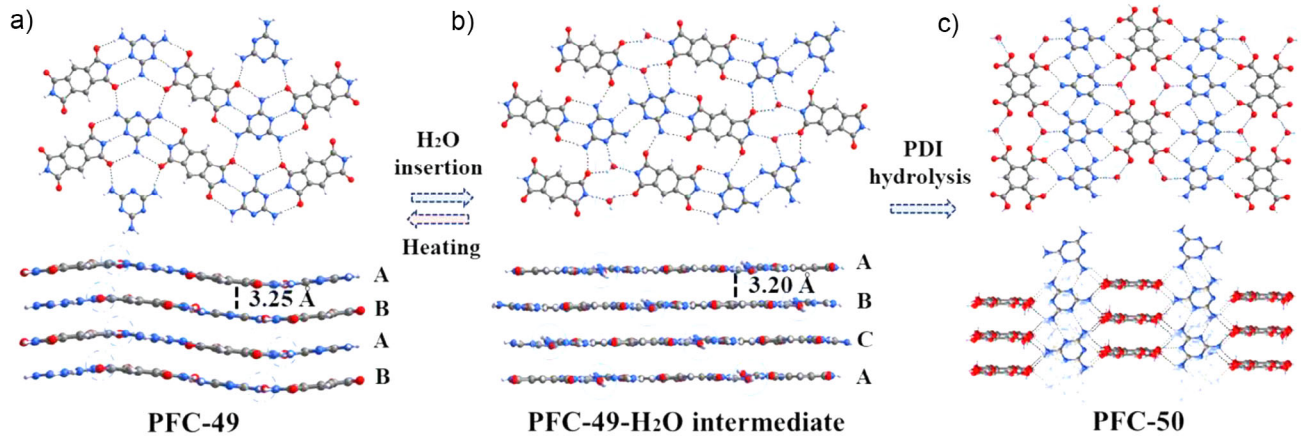

Figure 2. The single crystal structure of a) PFC-49, b) PFC-49-H_2O, and c) PFC-50 viewed along *a*-axis (upper panel) and *b*-axis (lower panel). The position adopting water from the surrounding environment is marked with dashed circles, and the carboxylic acids that stabilized water molecules through post-synthesis are marked with solid circles.

revealed that PFC-49 crystallizes in monoclinic space group $P2_1/n$. As shown in Figures 2a and S1, each PDI molecule connected with four neighboring melamine molecules via six N─H···O and two N─H···N hydrogen bonds (details of the hydrogen bonds are presented in Table S2), forming an undulated 2D supramolecular monolayer. These monolayers stack in an ABAB pattern, with π–π interactions between the aromatic backbone of PDI and the triazine ring of melamine along the *a*-axis, at a distance of 3.25 Å.

Since the PDI monomer can undergo ring-opening reactions to form pyromellitic acid (PMA) (Figure S22 and Scheme S1), it underwent a similar reaction, which was accompanied by a structural transformation from PFC-49 to PFC-50. Fortunately, we have successfully captured the intermediate (PFC-49-H_2O) through a single-crystal to single-crystal process[25–27] (Figure S4) and conclusively determined its structure via single-crystal X-ray diffraction. The crystal structure of PFC-49-H_2O clearly shows that water molecules exclusively insert into the hydrogen bonds where the layer undulation occurs, which is considered the place with maximum surface energy in an ultrathin layer.[28,29] As a result, half of the PDI and melamine hydrogen bonds were replaced by PDI and H_2O hydrogen bonds (Figure 2b, upper panel), and the undulated 2D layers evolved to planer layers (Figure 2b, lower panel). As shown in the electron density difference map of PFC-49-H_2O, the carbon atoms (C23 and C36) in the imide group connected with H_2O are more positively charged, while the oxygen atoms (O1 and O3) are more negatively charged (Figure 3a, right), in contrast to C28 and C31 (O2 and O4) of the imide group that bond with

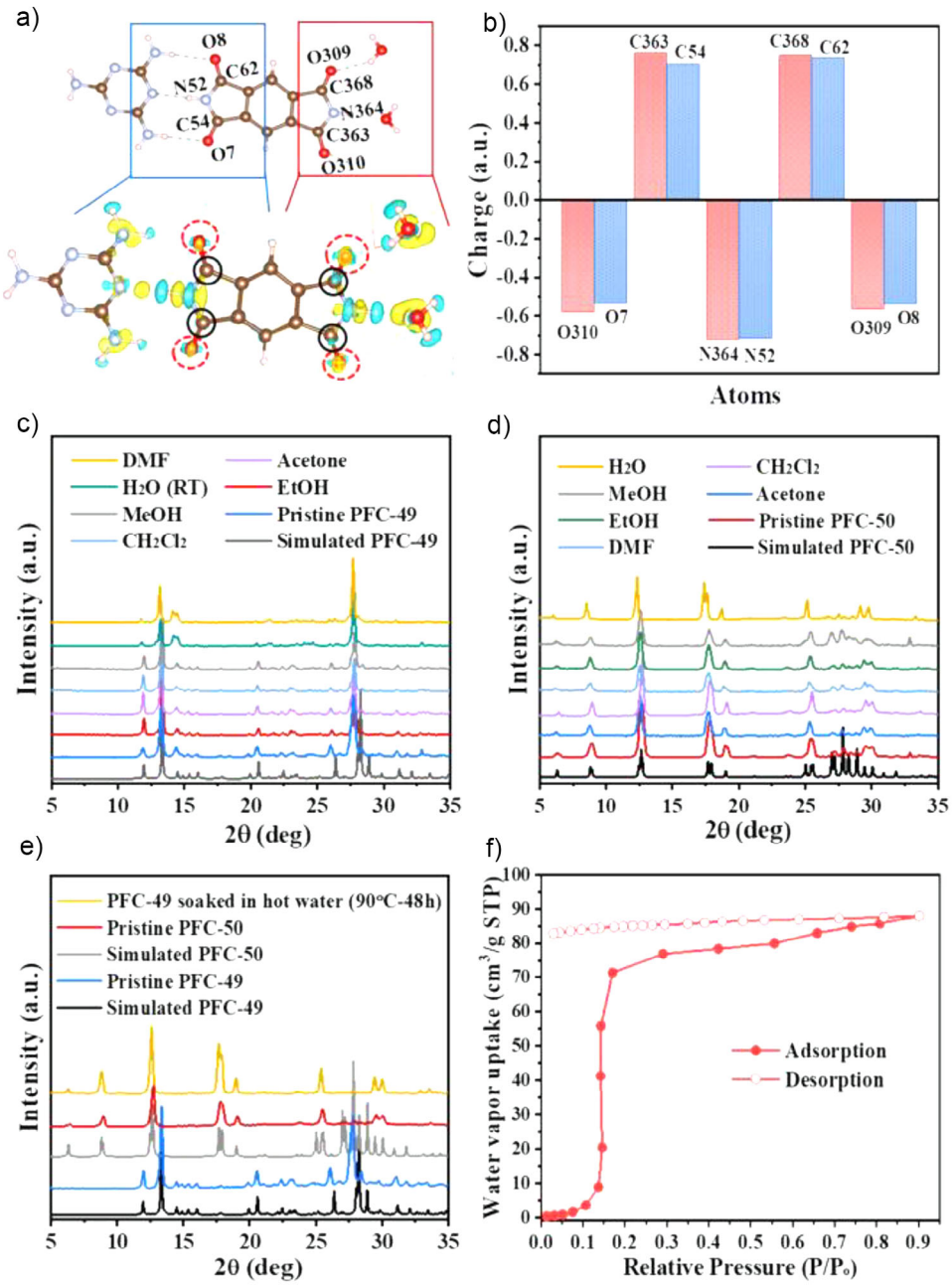

Figure 3. a) Charge density difference diagram for PFC-49-H_2O. Yellow and green contours represent electron accumulation and depletion, respectively. b) The Minimal Basis Iterative Stockholder (MBIS) atomic charge population analysis of atoms connected with H_2O (red) or melamine (blue) through hydrogen bonding in PFC-49-H_2O (the atom labels are shown in a), respectively. c and d) PXRD patterns of PFC-49 and PFC-50 before and after being treated with different solvents. e) PXRD patterns of PFC-49 before and after being soaked in hot water (90 °C) for 48 h. f) Water vapor adsorption and desorption isotherms of activated PFC-50 at 298 K.

melamine (Figure 3a, left). This observation is consistent with the results of Minimal Basis Iterative Stockholder (MBIS) and Hirshfeld-I atomic charge population analysis (Figures 3b and S23). These results suggest that the insertion of the water molecules increases the polarity of the imide groups, which would facilitate the subsequent deamidation reaction associated with the nucleophilic attack of carbonyl carbon by the oxygen atom in the water molecule. Moreover, it is worth mentioning that the PXRD pattern of PFC-49-H_2O, after heating at 150 °C for 4 h, is consistent with that of the as-synthesized PFC-49 (Figure S25). This indicates PFC-49-H_2O can be reversibly transformed back to PFC-49 upon heating.

Further extending the reaction time in hot water, PFC-49-H_2O was gradually transformed to PFC-50 through a dissolution–recrystallization process (Figure S4).[27] Single-crystal X-ray diffraction shows that PFC-50 crystallized in the triclinic system with space group P-1 (Table S1). As shown in Figures 2c and S3, the PDI molecules have completely

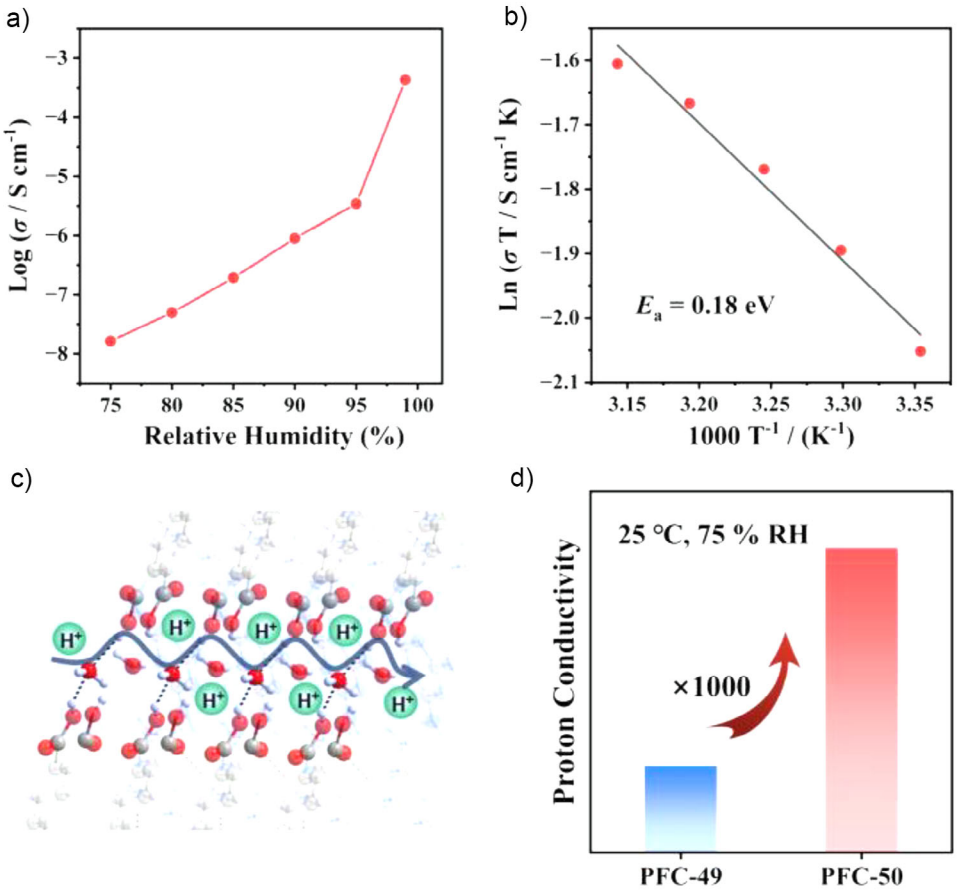

Figure 4. a) Proton conductivity (σ) of PFC-50 at 25 °C under different RH; b) Arrhenius plot of PFC-50 at varying temperatures and 99% RH. c) Illustration of the long-range proton conduction pathway in PFC-50. d) Comparison of proton conductivity between PFC-49 and PFC-50 at 75% RH and 25 °C.

transformed into their hydrolysis product PMA, which is connected with melamine and H_2O molecules through multiple hydrogen bonds, resulting in a 3D architecture. It is interesting to note that the carboxylic acids generated in PFC-50 stabilize H_2O molecules and form a 1D water channel along the *a*-axis, similar to the proton transport channel in CcO. As shown in Figures 1 (lower panel) and S3, each 1D channel comprises two water chains, in which every water molecule was stabilized by two adjacent carboxyl groups, occupying 6.6% of the total mass according to crystallographic data and thermogravimetric analysis (Figure S11). In addition, it should be noted that the direct self-assembly of PMA and melamine cannot yield the same structure as PFC-50, indicating that post-synthesis is essential for creating a 1D channel with exposed carboxylic acids for anchoring water molecules.

The chemical stability of PFC-49 and PFC-50 was carefully confirmed by powder X-ray diffraction (PXRD). As shown in Figures 3c,d, S6, and S8, both the PXRD patterns of PFC-49 and PFC-50 are in accordance with the simulated patterns derived from their single-crystal X-ray diffraction and can maintain the structural integrity after being soaked in various solvents and aqueous solutions (pH 2–10) for 2 days. However, immersing PFC-49 in hot water for 48 h resulted in a complete structure transformation to PFC-50, with no further change being detected (Figures 3e and S10). In addition, the water vapor adsorption isotherm (Figure 3f) of activated PFC-50 shows a steep increase in water uptake at low pressures ($P/P_0 = 0.1$–0.2), demonstrating its high affinity toward water molecules.[30] Moreover, the adsorbed water molecules cannot be completely removed even under very low pressure as shown in the desorption branch of isotherm. These results suggest that water molecules can be firmly stabilized by the exposed carboxylic acids in the channel of PFC-50 and form continuous 1D water channels that are promising as proton hopping paths.

Proton conductivity of PFC-49 and PFC-50. The proton conductivity of pelletized PFC-49 and PFC-50 was measured using AC impedance method, with PFC-49′s assessment limited to 75% relative humidity (RH) due to its structural transformation into PFC-49-H_2O in high humidity. As shown in Figure S14, when the temperature rises from 25 to 45 °C, the proton conductivity of PFC-49 increases from 1.58×10^{-11} to 9.07×10^{-11} S cm^{-1}. Utilizing the Arrhenius equation $\sigma T = A \exp(-E_a/k_B T)$, where k_B represents the Boltzmann constant and A is the pre-exponential factor, the activation energy (E_a) was calculated to be 0.73 eV. This value indicates a vehicle mechanism ($E_a > 0.4$ eV). As humidity increases to 90% RH, PFC-49 partially converts to the metastable

PFC-49-H_2O (Figure S16), where large number of water molecules are involved in the hydrogen-bond network and therefore facilitate the proton conduction. This resulted in an increased conductivity of 1.37×10^{-5} S cm^{-1} at 45 °C, 99% RH (Figure S17).

The RH dependence of Nyquist plots of PFC-50 is illustrated in Figure S18, and the proton conductivity was estimated from an equivalent circuit model. As shown in Figure 4a, with increasing RH from 75% to 99% at 25 °C, the proton conductivity for PFC-50 increased from 1.64×10^{-8} to 4.31×10^{-4} S cm^{-1}. This increment can be ascribed to the presence of large amounts of water molecules that was stabilized by exposed carboxylic groups in the channels of structure and served as hopping sites for proton.[11,31] Besides, Figure S19 displays the temperature dependence of PFC-50′s conductivity, which steadily increased with temperature, reaching 6.31×10^{-4} S cm^{-1} at 45 °C. The calculated E_a was 0.18 eV (Figure 4b), suggesting a Grotthuss mechanism ($E_a < 0.4$ eV)[32] with protons effectively jumping through the 1D hydrogen-bonded chains (Figure 4c). Consistent proton conductivity was observed throughout repeated measurements (Figure S20), and the PXRD remained unchanged after multiple cycles (Figure S21), demonstrating the excellent structural stability and reliable performance of PFC-50 even in the harsh environment of high humidity and fluctuating temperature.

Compared to PFC-49, PFC-50 shows significant improvement in proton conductivity (Figure 4d), which is attributed to the presence of exposed carboxylic acid groups after post-synthesis and the 1D water molecule chains stabilized in the structure, resembling the proton transport D-channel in CcO. The exposed carboxylic acid groups of the PMA molecules in PFC-50, with their acidic hydroxyls acting as proton donors and carbonyls as acceptors, enable rapid proton movement and enhanced conduction efficiency, resulting in a three-orders-of-magnitude improvement in proton conductivity.

In summary, we demonstrated a post-synthetic strategy to construct biomimetic proton transport channels in HOFs. A linear PDI precursor was assembled with melamine molecules to synthesize an HOF PFC-49. The obtained HOF underwent a structural transformation to PFC-50 upon treatment with water, in which the PDI molecules were converted into exposed carboxylic acids and stabilized water molecules to form proton channels in the structure. The constructed biomimetic proton channels demonstrated a significant enhancement in proton conductivity, increasing by three orders of magnitude at 75% RH and 25 °C. This innovative approach provides new ideas and strategies for the future design of biomimetic proton-conducting materials.

Supporting Information

The data that support the findings of this study are available in the Supporting Information of this article. Detailed information regarding the experimental methods, syntheses, crystallographic data, time-dependent PXRD data of PFC-49 to track the structural transformation process in both water and water vapor, TGA curves, N_2, CO_2, and water vapor sorption isotherms, water contact angle, and the DFT calculations.

Accession Codes: CCDC 2393251, 2393252, and 2393253 contain the supplementary crystallographic data of PFC-49, PFC-49-50, and PFC-49-H_2O. These data can be obtained free of charge via www.ccdc.cam.ac.uk/data_request/cif.

Acknowledgements

This work was financially supported by the CAS Youth Interdisciplinary Team (grant no. JCTD-2022-12), the Natural Science Foundation of Fujian Province (grant no. 2024J010040), and the National Natural Science Foundation of China (grant no. 22325109, 22405274, 22171263, 62227815). Fujian Science and Technology Innovation Laboratory for Optoelectronic Information of China (grant no. 2021ZR101), Self-deployment Project Research Program of Haixi Institutes, Chinese Academy of Sciences (grant no. CXZX-2022-GH09, CXZX-2023-GS03), and China Postdoctoral Science Foundation (grant no. GZB20240748). The authors would like to acknowledge Dr. Duan-Hui Si (FJIRSM, CAS) for his help in theoretical calculation and Dr. A.R. Mahammed Shaheer (FJIRSM, CAS) for his help in revising the manuscript.

Conflict of Interests

The authors declare no conflict of interest.

Data Availability Statement

The data that support the findings of this study are available in the Supporting Information of this article.

Keywords: Biomimetic proton channels · Hydrogen-bonded organic framework · Post-synthesis · Proton conduction

[1] T. Gensch, J. Heberle, C. Viappiani, *Photochem. Photobiol. Sci.* **2006**, *5*, 529–530.
[2] A. Migliore, N. F. Polizzi, M. J. Therien, D. N. Beratan, *Chem. Rev.* **2014**, *114*, 3381–3465.
[3] A. P. Demchenko, *BBA Adv.* **2023**, *3*, 100085.
[4] P. A. Peter Brzezinski, *J. Bioenerg. Biomembr.* **1998**, 30.
[5] K. Faxén, G. Gilderson, P. Ädelroth, P. Brzezinski, *Nature* **2005**, *437*, 286–289.
[6] J. P. Hosler, S. Ferguson-Miller, D. A. Mills, *Annu. Rev. Biochem.* **2006**, *75*, 165–187.
[7] H. J. Lee, E. Svahn, J. M. Swanson, H. Lepp, G. A. Voth, P. Brzezinski, R. B. Gennis, *J. Am. Chem. Soc.* **2010**, *132*, 16225–16239.
[8] T. Yamashita, G. A. Voth, *J. Am. Chem. Soc.* **2012**, *134*, 1147–1152.
[9] Y. Sun, J. Wei, Z. Fu, M. Zhang, S. Zhao, G. Xu, C. Li, J. Zhang, T. Zhou, *Adv. Mater.* **2023**, *35*, e2208625.
[10] S. C. Pal, D. Mukherjee, R. Sahoo, S. Mondal, M. C. Das, *ACS Energy Lett.* **2021**, *6*, 4431–4453.
[11] D. W. Lim, M. Sadakiyo, H. Kitagawa, *Chem. Sci.* **2019**, *10*, 16–33.

[12] S. Chen, Y. Ju, H. Zhang, Y. Zou, S. Lin, Y. Li, S. Wang, E. Ma, W. Deng, S. Xiang, B. Chen, Z. Zhang, *Angew. Chem. Int. Ed.* **2023**, *62*, e202308418.
[13] A. Karmakar, R. Illathvalappil, B. Anothumakkool, A. Sen, P. Samanta, A. V. Desai, S. Kurungot, S. K. Ghosh, *Angew. Chem. Int. Ed.* **2016**, *55*, 10667–10671.
[14] I. Hisaki, C. Xin, K. Takahashi, T. Nakamura, *Angew. Chem. Int. Ed.* **2019**, *58*, 11160–11170.
[15] R. B. Lin, Y. He, P. Li, H. Wang, W. Zhou, B. Chen, *Chem. Soc. Rev.* **2019**, *48*, 1362–1389.
[16] Q. Yin, P. Zhao, R.-J. Sa, G.-C. Chen, J. Lü, T.-F. Liu, R. Cao, *Angew. Chem. Int. Ed.* **2018**, *57*, 7691–7696.
[17] X. Y. Gao, Y. Wang, E. Wu, C. Wang, B. Li, Y. Zhou, B. Chen, P. Li, *Angew. Chem. Int. Ed.* **2023**, *62*, e202312393.
[18] X. Chen, R. K. Huang, K. Takahashi, S. I. Noro, T. Nakamura, I. Hisaki, *Angew. Chem. Int. Ed.* **2022**, *61*, e202211686.
[19] T. Steiner, *Angew. Chem. Int. Ed.* **2002**, *41*, 48–76.
[20] R. Sahoo, S. Mondal, S. C. Pal, D. Mukherjee, M. C. Das, *Adv. Energy Mater.* **2021**, *11*, 2102300.
[21] W. J. Phang, H. Jo, W. R. Lee, J. H. Song, K. Yoo, B. Kim, C. S. Hong, *Angew. Chem. Int. Ed.* **2015**, *54*, 5142–5146.
[22] S. Catak, G. Monard, V. Aviyente, M. F. Ruiz-López, *J. Phys. Chem. A* **2009**, *113*, 1111–1120.
[23] S. Antonczak, M. F. Ruiz-Lopez, J. L. Rivail, *J. Am. Chem. Soc.* **1994**, *116*, 3912–3921.
[24] J. A. Duffy, J. A. Leisten, *Nature* **1956**, *178*, 1242–1243.
[25] X. Chen, Z. Zhang, J. Chen, S. Sapchenko, X. Han, I. Da-Silva, M. Li, I. J. Vitorica-Yrezabal, G. Whitehead, C. C. Tang, K. Awaga, S. Yang, M. Schröder, *Chem. Commun.* **2021**, *57*, 65–68.
[26] S. Nakatsuka, Y. Watanabe, Y. Kamakura, S. Horike, D. Tanaka, T. Hatakeyama, *Angew. Chem. Int. Ed.* **2020**, *59*, 1435–1439.
[27] Y. Xiang, S. Wei, T. Wang, H. Li, Y. Luo, B. Shao, N. Wu, Y. Su, L. Jiang, J. Huang, *Coord. Chem. Rev.* **2025**, *523*, 216263.
[28] Y. L. Li, E. V. Alexandrov, Q. Yin, L. Li, Z. B. Fang, W. Yuan, D. M. Proserpio, T. F. Liu, *J. Am. Chem. Soc.* **2020**, *142*, 7218–7224.
[29] J. C. Meyer, A. K. Geim, M. I. Katsnelson, K. S. Novoselov, T. J. Booth, S. Roth, *Nature* **2007**, *446*, 60–63.
[30] N. C. Burtch, H. Jasuja, K. S. Walton, *Chem. Rev.* **2014**, *114*, 10575–10612.
[31] J. Lu, Y. Yoshida, M. Maesato, H. Kitagawa, *Angew. Chem. Int. Ed.* **2022**, *61*, e202213077.
[32] D. W. Lim, H. Kitagawa, *Chem. Rev.* **2020**, *120*, 8416–8467.

Manuscript received: February 23, 2025
Revised manuscript received: March 14, 2025
Accepted manuscript online: March 14, 2025
Version of record online: ■■, ■■

Communication

Organic Materials

Y.-L. Li, J.-F. Lu, Q. Yin, L. Cai, H.-J. Jiang, C. Liu, G. Xu*, T.-F. Liu* —— **e202504396**

Constructing Biomimetic Channels in Hydrogen-Bonded Organic Framework via Post-Synthesis for Enhanced Proton Conductivity

Proton transport in biological systems relies on amino acid residues with hanging carboxylic acids as proton donors and acceptors. Here, we first demonstrate that post-synthesis can create unoccupied carboxylic acid groups in HOFs, stabilizing water molecules and forming continuous proton channels. This strategy achieves 1000-fold enhancement in proton conductivity and the structure transformation was clearly revealed by crystallography.